International Journal of Mechanics and Energy (IJME)
Vol. 3, Issue 2, 2015, ISSN: 2286-5845

Evaluating the performance of two eddy-viscosity turbulence models to predict airflow and Local Mean Age of air

Guilherme Anrain Lindner [a]*, Karim Limam [a], Lelia POPESCU [b], Brahim BENHAMOU [c]

[a] *Laboratory of engineering sciences for environment (LaSIE), University of La Rochelle, France*

[b] *UTCB, Technical University of Construction of Bucharest, Lacul Tei Blvd, ROMANIA*

[c] *Laboratoire EnR2E, (CNEREE), Université Cadi Ayyad, Marrakech, Maroc*

Abstract: The goal of this work is to investigate the performance of two eddy-viscosity turbulence models, standard k-ε and SST k-ω, in predicting the two-dimensional airflow in a rectangular room and the local mean age of air using an open-source simulation tool, OpenFOAM. Two geometries were analyzed: the room used in the first case (Bartak, 2001), which consists of a lateral air entrance and an outlet on the top of the opposite side, and the experimental room from the second case (Annex 20 room by Nielsen, 1990), which represents a large rectangular room where the air is supplied horizontally on the upper left and is exhausted through the opening on the lower right of the opposite side. The velocity profiles and local mean age of air were analyzed in both cases.

Key words: Computational Fluid Dynamics, indoor airflow, standard k-ε, SST k-ω, local mean age.

1. Introduction

Airflow studies in closed environments are crucial to thermal comfort and the concentration of pollutants. Most respiratory diseases can be prevented simply by proper air circulation, and even industrial accidents can be prevented by inhibiting the accumulation of flammable gases. Many tools are currently available to minimize these effects, to predict the pattern of air circulation and improve the overall quality of air in any ambient. Tracer gas experiments have been widely employed for quantifying building ventilation performance, but the difficulty to change layouts and the costs makes it a little inconvenient. The most popular tool is the Computational Fluid Dynamic (CFD). The CFD can be used with a series of turbulence models in indoor cases to achieve, with a cost-effective simulation, trusted results. Combining both numerical and experimental tests, we can achieve a good accuracy and a great cost-benefit.

The CFD tools have numerous applications and can be used from aerodynamic tests to even simulate leaks in hydraulic machines. To suit each case, a proper turbulence models needs to be chosen, because each one have its peculiarity and suggested applications.

The k-ε model is one of the most common turbulence models for CFD, although it does not perform well in cases of large adverse pressure gradients (Wilcox [1]). The Shear Stress Transport, SST k-ω, model was designed to give a highly accurate prediction of flow separation under adverse pressure gradients by the inclusion of transport effects into the formulation of the eddy-viscosity, switching its behavior between the k-ε and k-ω models. The SST k-ω model is an evolution of the k-ω model, that exhibits some sensitivity to freestream boundary conditions on ω. The k-ω model appears most reliable

*** Corresponding author:** Guilherme Anrain Lindner
E-mail: lindner.guilherme@gmail.com

and can simulate the expansion rates in the highly anisotropic cold case at the same magnitude order as the measurements (Zhai et al [2]).

A more effective analysis of a room's ventilation efficiency than by use of velocity profiles is obtainable by using the local mean age of air (LMA), which is a more sensitive parameter for highlighting areas with inadequate ventilation, and thus for assessing ventilation efficiency [3].

2. Model Description

2.1. Governing equations

Reynolds [4] decomposed the Navier-Stokes equations into two parts, one related to the average value of the velocity vector and another related to its fluctuation, and applied the time average operator to study turbulent flows. The resulting set of equations is known as Reynolds Average Navier-Stokes (RANS) equations and gives information about the mean flow.

Although this approach is not able to describe the multitude of length scales involved in turbulence, it has been largely used worldwide, since the gained information in relation to the mean flow is satisfactory.

Considering that the variation of density and viscosity are small enough that their effects on turbulence can be ignored, and the fluid is Newtonian, incompressible, the governing RANS equations in Cartesian coordinates can be expressed by Versteeg and Malalasekera [5]:

$$\frac{\partial U_i}{\partial x_i} = 0 \tag{1}$$

$$\rho \frac{\partial (U_i U_j)}{\partial x_j} = -\frac{\partial P}{\partial x_i} + \frac{\partial}{\partial x_j}\left(\mu \frac{\partial U_i}{\partial x_j} - \rho \overline{u_i u_j}\right) + F_i \tag{2}$$

where U_i and U_j are components of the average velocity vector [m/s], ρ is the fluid density [kg/m^3], μ is the dynamic viscosity of the fluid [Pa.s], P is the mean average pressure [Pa] and F_i is a component of the bulk force vector [N]. The extra term that appears in (2) compared to the original Navier-Stokes equations, $\overline{u_i u_j}$, is the product of fluctuation velocities [m^2/s^2] (termed Reynolds stresses) and is never negligible in any turbulent flow. It represents the increase in the diffusion of the mean flow due to the turbulence. Equations (1) and (2) can only be solved if the Reynolds stress tensor is known, a problem referred to as the 'closure problem' since the number of unknowns is greater than the number of equations.

The main goal of the turbulence studies based on the RANS equations is to determine the Reynolds stresses. According to Kolmogorov [6] they can be evaluated by the following expression:

$$-\overline{u_i u_j} = \nu_t \left(\frac{\partial U_i}{\partial x_j} + \frac{\partial U_j}{\partial x_i}\right) - \frac{2}{3}\delta_{ij} k \tag{3}$$

where δ_{ij} is the Kronecker delta and the kinetic energy of the turbulent motion, k, is defined as $k = \overline{u_i u_i}/2$ [m^2/s^2]. Substitution of Equation (3) into Equation (2) results in the average Navier-Stokes equations with the Reynolds stresses modeled via the viscosity concept,

$$\rho \frac{\partial (U_i U_j)}{\partial x_j} = -\frac{\partial P'}{\partial x_i} + \frac{\partial}{\partial x_j}\left[(\mu + \mu_t)\left(\frac{\partial U_i}{\partial x_j} + \frac{\partial U_j}{\partial x_i}\right)\right] + \rho\beta(T_0 - T)g_i \tag{4}$$

where μ_t is the turbulent viscosity, $P' = P + 2/3\,k$ is the modified pressure, β is the thermal expansion coefficient of air, T_0 is the temperature at a reference point, T is the temperature, and g is the gravity acceleration.

The last term on the right side of (4) is the buoyancy term.

The turbulent viscosity can be expressed as the product of a velocity scale, u [m/s], and a length scale, L_μ [m], $\mu_t = \rho u L_\mu$. Considering the velocity scale being calculated by $u = k^{12}$, Kolmogorov [6] and

Prandtl [7] independently proposed the following relation for the turbulent viscosity,

$$\mu_t=\rho c_\mu k^{1/2} L_\mu \quad (5)$$

where c_μ (=0.09) is an empiric constant.

To complete the set of equations described above, the most popular turbulence models define two other transport equations: one for the turbulent kinectic energy, *k*, and another for a variable that relates *k* to L_μ. These models are called two equation models, and two of them have been employed in this work: the standard *k*-ε model (Launder and Spalding, [8]) and the *k*-ω model (Wilcox [9]).

2.2. Two-equation turbulence model

Explicit formulations and descriptions of the three turbulence models, *k*-ε, *k*-ω and *SST k*-ω, are described below.

2.2.1. k-ε model

Due to its robustness, economy and acceptable results for a considerable amount of flows the k-ε model is the most commonly used model for numerical predictions of industrial flows, although it is known to have deficiencies in some situations involving streamline curvature, acceleration and separation. This model will be used in this research due to its position as the turbulence model most frequently used within the computational domain adopted in this work.

In this model, proposed by Launder and Spalding [8], the second variable for the complementary transport equations is the rate of the viscous dissipation, ε [m^2/s^3], which is related to *k* by:

$$\varepsilon=k^{3/2}/L \quad (6)$$

Therefore, the set of equations concerning the standard *k*-ε model is composed of Equations (1), (4), (5) and (6), and two transport equations for *k* and ε that are, respectively, given by:

$$\rho\frac{\partial(U_j k)}{\partial x_j}=\frac{\partial}{\partial x_j}\left[\left(\mu+\frac{\mu_t}{\sigma_k}\right)\frac{\partial k}{\partial x_j}\right] + \mu_t\left[\frac{\partial U_i}{\partial x_j}+\frac{\partial U_j}{\partial x_i}\right]\left[\frac{\partial U_i}{\partial x_j}\right]-\rho\varepsilon \quad (7)$$

$$\rho\frac{\partial(U_j \varepsilon)}{\partial x_j}=\frac{\partial}{\partial x_j}\left[\left(\mu+\frac{\mu_t}{\sigma_\varepsilon}\right)\frac{\partial \varepsilon}{\partial x_j}\right] + c_1\mu_t\frac{\varepsilon}{k}\left[\frac{\partial U_i}{\partial x_j}+\frac{\partial U_j}{\partial x_i}\right]\left[\frac{\partial U_i}{\partial x_j}\right]-c_2\rho\frac{\varepsilon^2}{k} \quad (8)$$

where c_1 = 1.42; c_2 = 1.92; σ_k = 1 e σ_ε = 1.22 are empirical constants.

As (7) and (8) cannot describe correctly the movement of the fluid near solid surfaces, the so called wall-functions are required to make it applicable to the entire domain.

2.2.2. k-ω model

To understand the SST *k*-ω model, we need to review the concepts of the *k*-ω model. Kolmogorov [6] proposed the first two-equation model of turbulence, which included one differential equation for *k* and a second for ω, defined as the rate of dissipation of energy per unit volume and time. Saffman [10] independently formulated a similar two-equation *k*–ω model. The parameter ω can be considered "a frequency characteristic of the turbulence decay process" [10] and is related to dissipation by

$$\omega=\frac{\varepsilon}{c_\mu^4 k} \quad (9)$$

Wilcox and Alber [11] Saffman and Wilcox [12], and others cited in Wilcox [1] have provided further improvements to the model. The version of the *k*–ω model presented by [9], who formulated a low Reynolds number alternative to the standard *k*-ε turbulence model, is used here.

Wilcox [9] proposed that the dissipation-rate equation of the *k*-ε model be replaced by an equation for a specific dissipation rate defined as $\omega = k/\varepsilon$. This *k*-ω model predicts the behaviour of attached boundary layers in adverse pressure gradients more

accurately than *k*-ε models, but performs poorly in free shear flows (Bardina et al. [13]). The vorticity, ω, is associated to the turbulent kinetic energy, *k*, by the following expression:

$$\mu_t = \rho \frac{k}{\omega} \tag{10}$$

Thus, in the model proposed by Wilcox [9] the transport equations for the turbulent kinetic energy *k* and the specific dissipation rate ω are defined by (12) and (13), respectively,

$$\rho \frac{\partial (U_j k)}{\partial x_j} = \frac{\partial}{\partial x_j}\left[\left(\mu + \frac{\mu_t}{\sigma_k}\right)\frac{\partial k}{\partial x_j}\right] + \mu_t\left[\frac{\partial U_i}{\partial x_j} + \frac{\partial U_j}{\partial x_i}\right]\left[\frac{\partial U_i}{\partial x_j}\right] - \beta_1 \rho k \omega \tag{11}$$

$$\rho \frac{\partial (U_j \omega)}{\partial x_j} = \frac{\partial}{\partial x_j}\left[\left(\mu + \frac{\mu_t}{\sigma_\omega}\right)\frac{\partial \omega}{\partial x_j}\right] + \alpha \mu_t \frac{\omega}{k}\left[\frac{\partial U_i}{\partial x_j} + \frac{\partial U_j}{\partial x_i}\right]\left[\frac{\partial U_i}{\partial x_j}\right] - \beta_2 \rho \omega^2 \tag{12}$$

where $\sigma_k = 2$, $\sigma_\omega = 2$, $\beta_1 = 0.09$, $\beta_2 = 0.075$ and $\alpha = 5/9$.

The main problem with the Wilcox model is its well known strong sensitivity to the free stream values of ω. Depending on the value specified for ω at the inlet, a significant variation in the results of the model can be obtained. A possible solution to this deficiency is to use a combination of the *k*-ω model equations implemented near wall regions and the *k*-ε turbulence model to be employed in the bulk flow region. This leads Menter [14] to formulate the Shear-Stress Transport (SST) turbulence model that is covered in the next section.

To close the set of equations presented above and to determine the temperature distribution and the buoyancy term in Equation (4), the conservation of energy must be solved,

$$\rho \frac{\partial (U_j T)}{\partial x_j} = \frac{\partial}{\partial x_j}\left[\tau_{T,\text{eff}} \frac{\partial T}{\partial x_j}\right] + \dot{q}/C_p \tag{13}$$

where $\tau_{T,eff}$ is the effective turbulent diffusion coefficient for *T*, $\dot{q}$ is the thermal source, and C_p is the specific heat.

2.2.3. SST k-ω model

The SST k-ω turbulence model is a two-equation eddy-viscosity model, which has become very popular. The shear stress transport (SST) formulation combines the best of the two turbulence models, *k*-ε and *k*-ω. The use of a k-ω formulation in the inner parts of the boundary layer makes the model directly usable all the way down to the wall through the viscous sub-layer; hence, the SST *k*-ω model can be used as a Low-Re turbulence model without any extra damping functions. The SST formulation also switches to a *k*-ε behaviour in the free-stream and thereby avoids the common *k*-ω problem whereby the model is too sensitive to the inlet free-stream turbulence properties.

Authors who use the SST *k*-ω model often merit it for its reliable behaviour in adverse pressure gradients and separating flow. The SST *k*-ω model produces strong turbulence levels in regions with large normal strain, such as regions of stagnation and regions with strong acceleration. This tendency is much less pronounced than with a normal *k*-ε model however.

3. Numerical Methodology

3.1. Software

The numerical solution of the governing equations was performed using the opensource computational fluid dynamics code OpenFOAM, version 2.2.0 (2013). In this code, the conservation equations for mass, momentum and turbulence quantities are solved using the finite volume discretisation method.

To couple the Navier-Stokes equations, the SIMPLE algorithm (Semi-Implicit Method for Pressure-Linked Equations) is implemented on OpenFOAM with an iterative procedure, which can be summed up as follows:

1. Set the boundary conditions.
2. Solve the discretised momentum equation to compute the intermediate velocity field.

3. Compute the mass fluxes at the cell faces.
4. Solve the pressure equation and apply under-relaxation.
5. Correct the mass fluxes at the cell faces.
6. Correct the velocities based on the new pressure field.
7. Update the boundary conditions.
8. Repeat until convergence occurs.

The code of OpenFOAM is a free and openly available source software under GNU General Public License, enabling anybody to adjust the code in order to explore all of its capacities.

In this work, we adjusted the SimpleFoam solver to allow us to track the local mean age of air, as described in section 3.2.

3.2. Studied Cases

Here the two studied cases are presented: the 3D case from [15] and the 2D model from the [16] geometry.

3.2.1. Case 1 – Bartak

The first case (Fig. 1) has a simple tridimensional geometry with a lateral inlet and an outlet on the top of the opposite side, as used by [15]. The dimensions of the rectangular room are 4 m long, 3.6 m wide and 3 m tall. The inlet is 0.3 m x 0.2 m and is placed in the middle plane of the left wall, 2.05 m from the floor. The outlet is located on the top wall, close to the east wall.

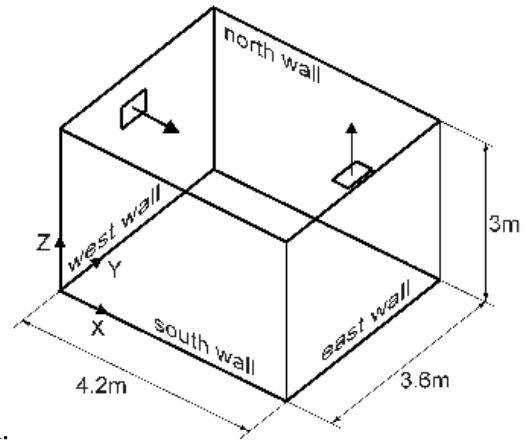

Fig. 1: Case 1 geometry (bartak experimental case)

The velocity at the inlet is 1.68 m/s and at the outlet, pressure is fixed to 0 Pa. All the walls have the nonslip condition, where $U_x = U_y = U_z = 0$.

The computational mesh (Fig. 2) used for both turbulence models is identical, with 52288 elements.

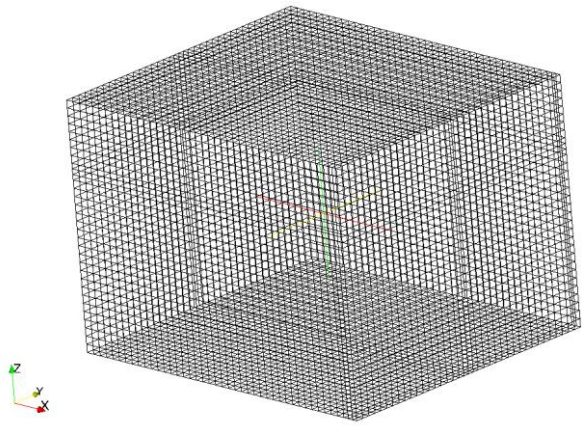

Fig. 2: Computational mesh for Case 1

Since the 3D model requires a bigger mesh compared to the 2D model, the mesh has not been refined so as to enable us to view the behaviour of both models on a course mesh.

3.2.2. Case 2 – Annex 20

Case 2 consists of an isothermal room named Annex 20, presented by [16]. In the test room of Annex 20, air is supplied to the horizontal top left, and out through the opening in the bottom right. This experimental room was designed to represent a 2D model, where its inlet and outlet occupies the whole depth of the room. Picture 3 shows a sketch of the experimental device:

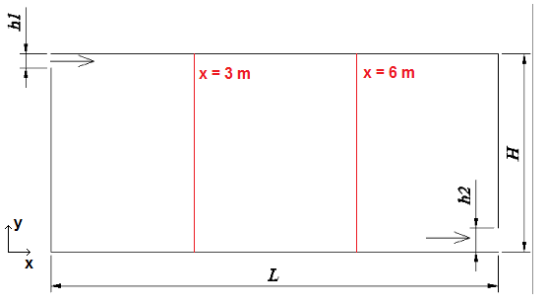

Fig. 3: Case 2 - Annex 20 sketch

where L = 9m, H = 3m, h_1 = 0.168m and h_2 = 0.48m. The red line represents the data collected for the results.

The boundary conditions for Case 2 are: U_x = 0,455 m/s, and $U_y = U_z = 0$. The outlet pressure is fixed at 0 Pa. The computational mesh used in this case is hexahedral and consists of 18720 elements, shown in Fig. 4.

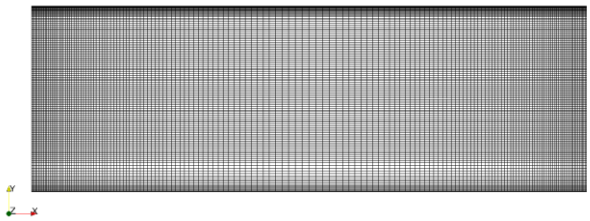

Fig. 4: Computational mesh for Case 2

The mesh on the walls and the inlet area has been gradually refined.

The convergence criteria for both cases are set to an average error of less than 1e-5.

3.3. Ventilation Efficiency

In order to analyse room ventilation efficiency, the local mean age of air is used, which can be described as follows:

The local mean age of air :

$$\varepsilon_p = \frac{\bar{\tau}_p}{\bar{\tau}_n} \tag{14}$$

is the average residence time of air in the local area (also called the recirculation time or the inverse of renew rate):

$$\bar{\tau}_n = \frac{V}{Q} = \frac{1}{R} \tag{15}$$

is the mean age of air in the p area (Fig. 5), or the average journey time of air from entering the local to the area p.

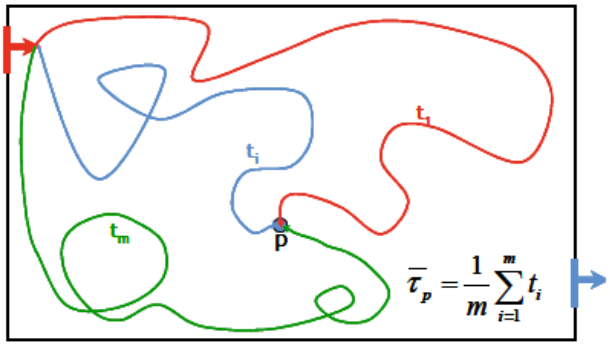

Fig. 5: Schema for the local mean age on point p (Ricciardi [17])

Where a large value of ε_p corresponds to a low value of $\bar{\tau}_p$ with respect to $\bar{\tau}_n$, then the renewal of the air in p is faster than the renewal of the entire local area, indicating a better renewal in this area (near the entrances for example). In contrast, in a poorly renewed "dead zone" area, this coefficient is low.

The calculation of the local mean age value is made by means of solving an additional partial differential equation. For numerical purposes the equation is derived from the concentration equation, known also as the 'passive scalar' equation (Equation (16)). This formulation does not interact with the velocity field.

$$\nabla(\rho\vec{U}\phi_i - \Gamma_i \nabla\phi_i) = S_{\phi_i} \tag{16}$$

Where ρ is the fluid density kg/m^3, Φ is the scalar, U the fluid velocity, Γ the diffusion coefficient and S_Φ is the source term. The value of the source term is normally equal to 1 [16].

The diffusion coefficient is given by the following relation:

$$\Gamma = \frac{\mu}{\sigma_l} + \frac{\mu_t}{\sigma_t} \tag{17}$$

Where μ, μ_t are the dynamic and turbulent viscosity and σ_l, σ_t are the laminar and turbulent Schmidt Number.

These equations are implemented on the original solver of OpenFOAM to allow the calculation of the LMA.

4. Results and discussions

The numerical results from Case 1 and Case 2 are presented in this section. Both cases are tested with the two turbulence models.

4.1. Case 1 – Bartak

Case 1 was tested experimentally by Bartak and the LMA results were collected. No experimental results are available for velocity profiles on this case.

On Fig. 6 we can see the velocity profiles on the position x = 2,2 and x = 3,2, both on the XZ plane for the two turbulence models.

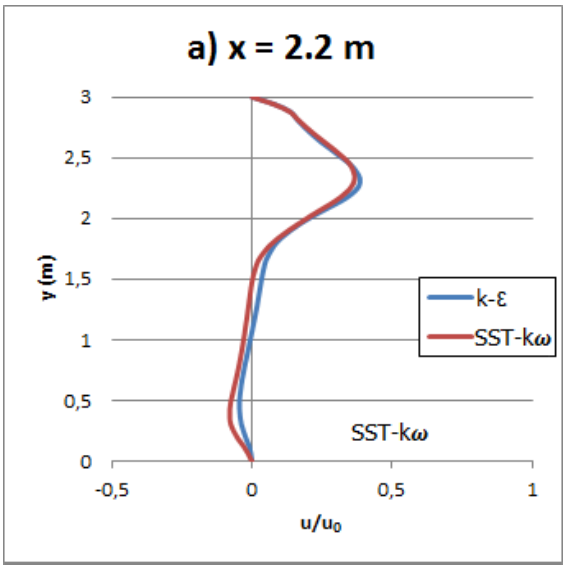

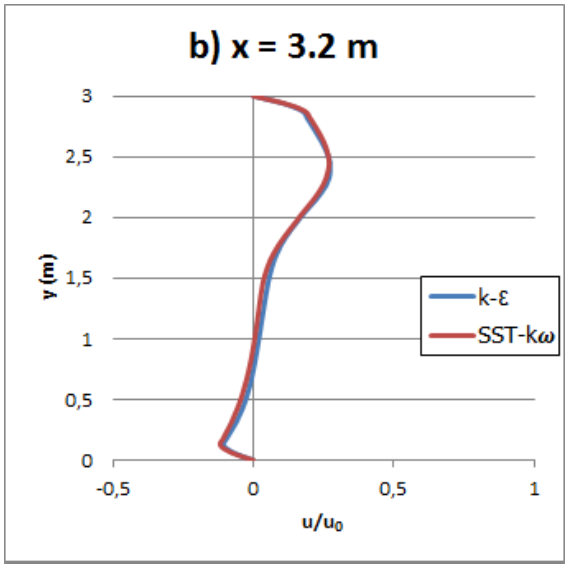

Fig. 6: Velocity profiles for both turbulence models -Case 1

The results are quite similar, with a mean squared error of 1.4% between the two models in the first position (a) and 0,8% in the second position.

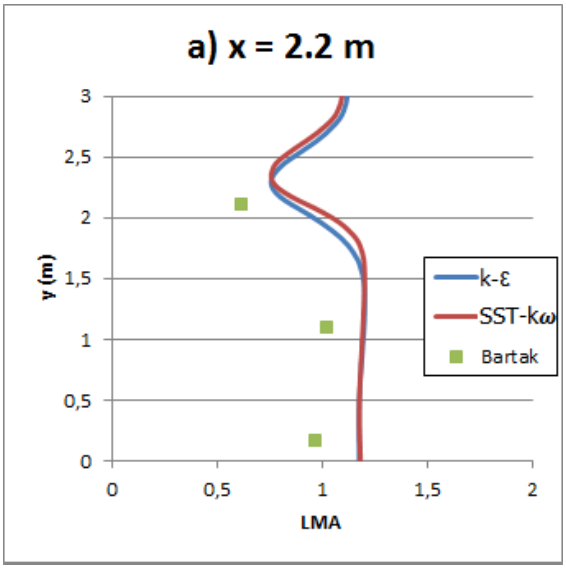

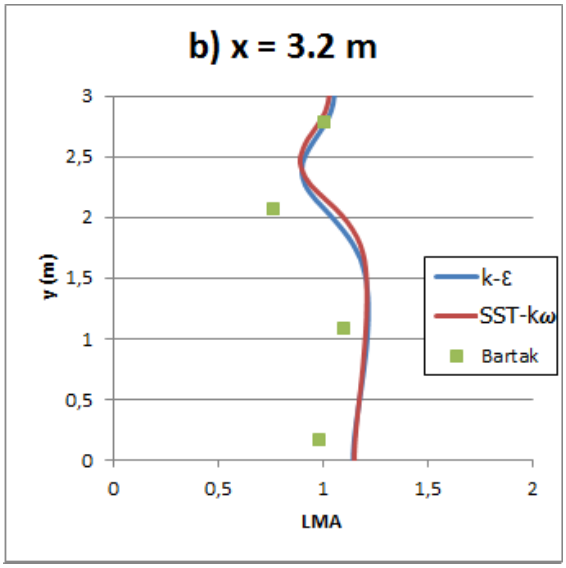

Fig. 7: LMA of the two turbulence models - Case 1

Fig. 7 compares the Local Mean Age for both positions (x = 2.2 m and x = 3.2 m) where we compare with the experimental results from [15]. Both turbulence models show similar results and the same tendency of the experimental data.

4.2. Case 2 – Annex 20

Reference [16] has collected experimental results of velocity profiles for the Annex 20 room.

On Fig. 8 we can see the velocity profiles on the X = 3,0 and X = 6,0, both on the XZ plane for the three turbulence models.

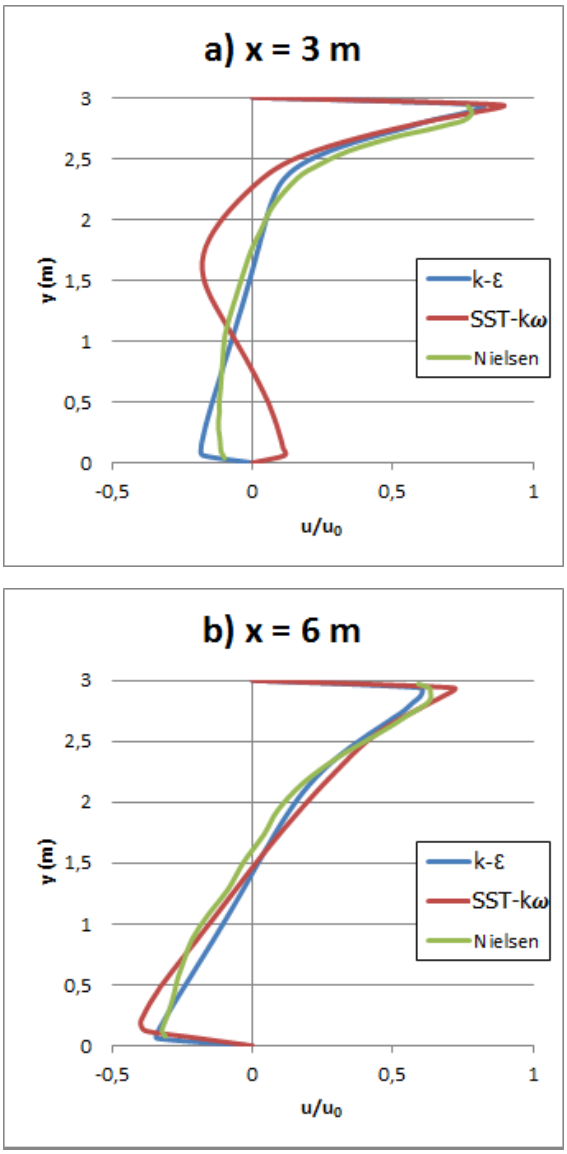

Fig. 8: Velocity profiles of the two turbulence models -Case

The second position (x = 6 m) show a good tendency for both models, close to the experimental results. The first position, closer to the inlet, exhibits peculiar behavior for the SST *k-ω* model. This situation occurs because of the appearance of a recirculation area, which is induced by the SST *k-ω* model.

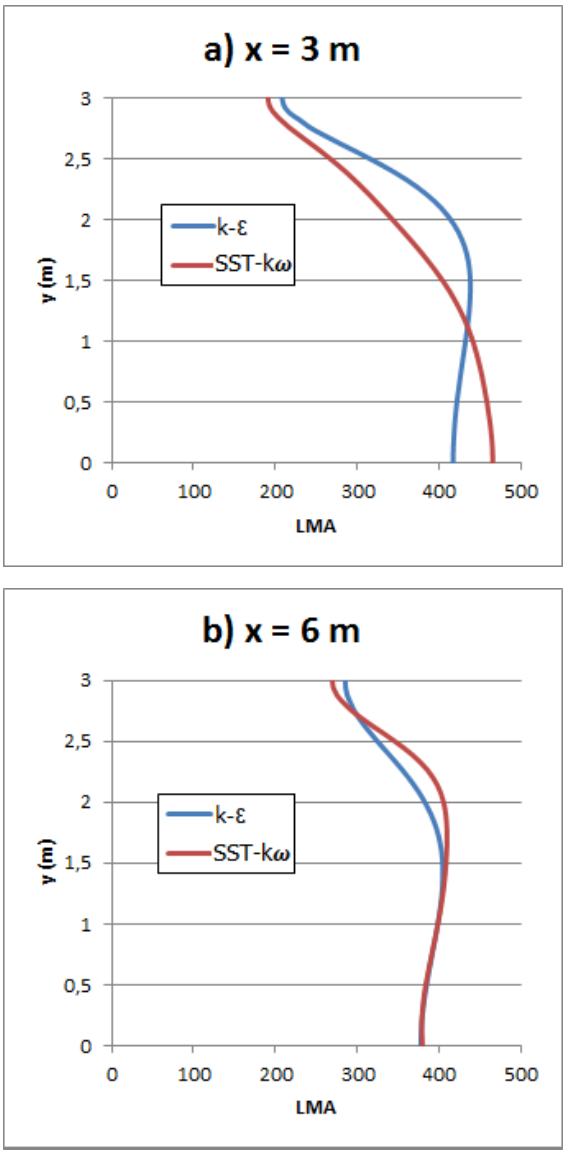

Fig. 9: LMA of the two turbulence models - Case 2

The LMA shown in Fig. 9 reflects the differences presented on the velocity profiles. In the second position, both models show the same tendency but in the first position different behaviours are evident because of the recirculation zones.

5. Conclusions

This article employed two turbulence models, standard k-ε and SST k-ω, to predict the two-dimensional airflow in a rectangular room as well as the local mean age of the air in two isothermal buildings. The computed results have been compared with experimental data from [16] for the Local Mean Age profiles and [17] for the velocity profiles. The performance of both models was acceptable for the first case, where no significant difference appeared in the LMA and velocity profile. This behaviour shows that the SST k-ω mainly used the k-ε formulation to solve it, not switching to the k-ω model because of the mesh refinement. For the room experiment, some differences appeared, particularly near the inlet, where strong recirculation appeared in the SST k-ω model. This phenomena appears because the SST k-ω model uses some k-ω characteristics for the freestream flow. The characteristic of the SST k-ω of being able to switch its behaviour between the k-ε and k-ω models gives great flexibility, but in this case it created a recirculation that did not exist, compared to the experimental results.

References

[1] Wilcox, D.C., 1998, Turbulence modeling for CFD. DCW Industries, Inc, La Canada, CA. p. 540.

[2] Zhai, Z., Zhang, Z., Zhang, W., Chen, Q., 2007, Evaluation of various turbulence models in predicting airflow and turbulence in enclosed environments by CFD: Part-1: summary of prevalent turbulence models. HVAC&R Research, Vol. 13, pp. 1-21.

[3] Chantelou, V., Mirade, P., 2009, Computational fluid dynamics (CFD) modelling of local mean age of air distribution in forced-ventilation food plants, Journal of Food Engineering, Vol. 90, pp. 90-103.

[4] Reynolds, O., 1895, On the dynamical theory of incompressible viscous fluids and the determination of the criterion, Phil. Trans. Roy. Soc. London A, Vol. 186, pp. 123-164.

[5] Versteeg, H. K. and Malalasekera, W., 1995, An introduction to computational fluid dynamics, Longman Scientific & Technical, New York.

[6] Kolmogorov, A.N., 1942, Equations of turbulent motion of an incompressible fluid. Izvestia Acad. Sci., USSR; Phys. Vol. 6, pp. 56–58.

[7] Prandtl, L., Wighardt, K., 1945, Über ein neues formelsystem für die ausgebildete turbulenz, Nachr. Akad. Wiss., Math.-Phys, Kl., 6.

[8] Launder, B. E. and Spalding, D. B., 1974, The numerical computation of turbulent flows, Comp. Meth. Appl. Mech. Energy, Vol. 3, pp. 269-289.

[9] Wilcox, D.C., 1988, Reassessment of the scale determining equation for advance turbulence models. AIAA Journal, Vol. 26, pp. 1299-1310.

[10] Saffman, P.G., 1970, A model for inhomogeneous turbulent flow. Proc. R. Soc., London A, Vol. 317, pp. 417–433.

[11] Wilcox, D.C. and Alber, I.E., 1972, A turbulence model for high speed flows. In: Proc. of the 1972 Heat Trans. & Fluid Mech. Inst., Stanford Univ. Press, Stanford, CA, pp. 231–252.

[12] Saffman And Wilcox 1974, Turbulence-model predictions for turbulent boundary layers, AIAA Journal, Vol 12, No. 4 (1974), pp. 541-546.

[13] Bardina, J. E., Huang, P. G. and Coakley, T. J., 1997, Turbulence modeling validation, testing, and development, *NASA-TM-110446.*

[14] Menter, F. R., 1992, Improved two-equation k-ω turbulence model for aerodynamic flows, NASA TM-103975, 1992.

[15] Bartak, 2001, Experimental and Numerical study of Local Mean Age of Air, Building Simulation, Seventh International IBPSA Conference.

[16] Nielsen, P. V., 1990, Specification of a two-dimensional test case, Technical report, International Energy Agency, Annex 20: Air Flow Pattern Within Buildings.

[17] Ricciardi, 2009, *Methode d'evaluation de la fonction surveillance assignee a la ventilation dans une installation à risques industriels*, DSU/SERAC/LEMAC/09-31.